

Magnetostriction in the Bose-Einstein Condensate quantum magnet $\text{NiCl}_2\text{-4SC}(\text{NH}_2)_2$

V. S. Zapf¹, V. F. Correa,^{2,†} C. D. Batista,³ T. P. Murphy², E. D. Palm², M. Jaime,¹ S. Tozer², A. Lacerda¹, A. Paduan-Filho⁴

¹National High Magnetic Field Laboratory (NHMFL), Los Alamos National Lab (LANL), Los Alamos, NM

²NHMFL, Tallahassee, Florida

³Condensed Matter and Thermal Physics, LANL, Los Alamos, NM

⁴Instituto de Física, Universidade de Sao Paulo, Brazil

[†] Now at Comisión Nacional de Energía Atómica, Centro Atómico Bariloche, 8400 S. C. de Bariloche, Argentina

(Dated: October 18, 2018)

The quantum magnet $\text{NiCl}_2\text{-4SC}(\text{NH}_2)_2$ is a candidate for observing Bose-Einstein Condensation of spin degrees of freedom in applied magnetic fields. An XY antiferromagnetic ordered state occurs in a dome-shaped region of the temperature-field phase diagram between $H_{c1} = 2.1$ T and $H_{c2} = 12.6$ T and below 1.2 K. BEC corresponds to the field-induced quantum phase transition into the ordered state. We investigate magnetostriction in single crystals of this compound at dilution refrigerator temperatures in magnetic fields up to 18 T, and as a function of magnetic field angle. We show that significant changes in the lattice parameters are induced by magnetic fields, and argue that these result from antiferromagnetic couplings between the Ni spins along the tetragonal c-axis. The magnetic phase diagram as a function of temperature, field, and field angle can be extracted from these data. We discuss the implications of these results to Bose-Einstein Condensation in this system.

PACS numbers:

Keywords:

I. INTRODUCTION

In recent years, there has been a surge of interest in the topic of quantum magnetism in condensed-matter systems. Nature and human ingenuity have provided us with a rich variety of spin structures including reduced-dimensional ladders, chains or planes, dimers, frustrated spins, and single-molecule magnets. These materials all share the common trait that quantum effects, such as spin fluctuations and quantized spin levels, play a significant role in shaping the ground state and the physical properties of the system. The resultant behavior can be complex and challenge our understanding, as well as provide potentially useful applications.

In particular, there have been a number of attempts recently to observe the quintessential quantum ground state Bose-Einstein Condensation (BEC) in quantum magnets. BEC was first observed in dilute gases of ^{87}Rb atoms,¹ leading to a nobel prize being awarded in 2001. It turns out that a form of BEC can also be observed in quantum magnets, e.g. crystalline lattices containing spins. BEC in quantum magnets was first predicted to occur in 1991 by Ian Affleck². In the past few years, several reports of BEC in real spin systems have been published including TiCuCl_3 ,^{3,4} $\text{BaCu}_2\text{SiO}_6$,^{5,6} CsCuCl_4 ,^{7,8} and $\text{NiCl}_2\text{-4SC}(\text{NH}_2)_2$.^{9,10}

The bosons that condense in these systems are not the atoms, but rather Cu or Ni spin degrees of freedom (also referred to as triplons or magnons in the literature.) The BEC corresponds to the onset of magnetic order induced by magnetic fields. Thus, the tuning parameter for inducing condensation in spin systems is not the temperature, but the magnetic field.

In this paper, we focus on the organic quantum magnet $\text{NiCl}_2\text{-4SC}(\text{NH}_2)_2$ (DTN). It is the first compound based on Ni (spin $S = 1$) instead of Cu ($S = 1/2$) and the first organic compound in which BEC has been observed.⁹ We present an extended introduction to the topic of Bose-Einstein condensation in DTN and then discuss new magnetostriction data for this compound at low temperatures.

The energy level diagram of the Ni system differs from those of the previously studied Cu systems. The Ni $S = 1$ spin triplet is split by single-ion anisotropy into a $S_z = 0$ ground state and $S_z = \pm 1$ excited states with an energy gap of $D \sim 10$ K.^{10,11,12} The $S_z = \pm 1$ levels are dispersed by the antiferromagnetic coupling J , e.g. the spins can have different energies depending on their orientation with respect to each other. Thus these levels become broad bands, as shown in Fig. 2 where the bottom of the band is the AFM $k = (\pi, \pi, \pi)$ vector. When a magnetic field is applied along the tetragonal c-axis, the Zeeman effect lowers the $S_z = 1$ level until the bottom of the band becomes degenerate with the $S_z = 0$ ground state at H_{c1} (see Fig. 2). Between H_{c1} and H_{c2} the mean-field ground state becomes a linear combination of all three energy levels until finally at H_{c2} the gap reopens now with the $S_z = 1$ level as the ground state.⁹

At zero field, the gap between the $S_z = 0$ and the $S_z = \pm 1$ levels precludes any magnetic order. However, between H_{c1} and H_{c2} , XY antiferromagnetic order occurs at low temperatures. The region of field-induced antiferromagnetic order between H_{c1} and H_{c2} and below the maximum $T_N = 1.2$ K is shown in the phase diagram in Fig. 1. At H_{c1} , the spins order antiferromagnetically in the a-b plane, perpendicular to the applied field direc-

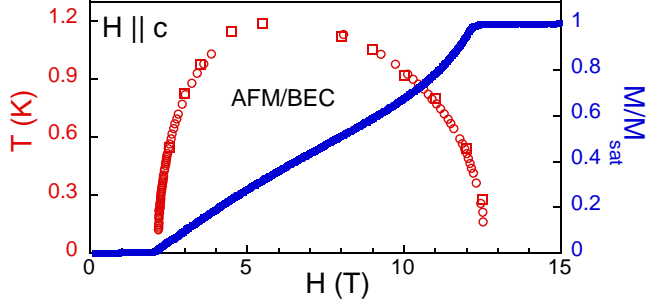


FIG. 1: Temperature T - Magnetic field H phase diagram for $H||c$ determined from specific heat and magnetocaloric data.⁹ The magnetization vs field at 16 mK is overlaid onto the phase diagram.¹²

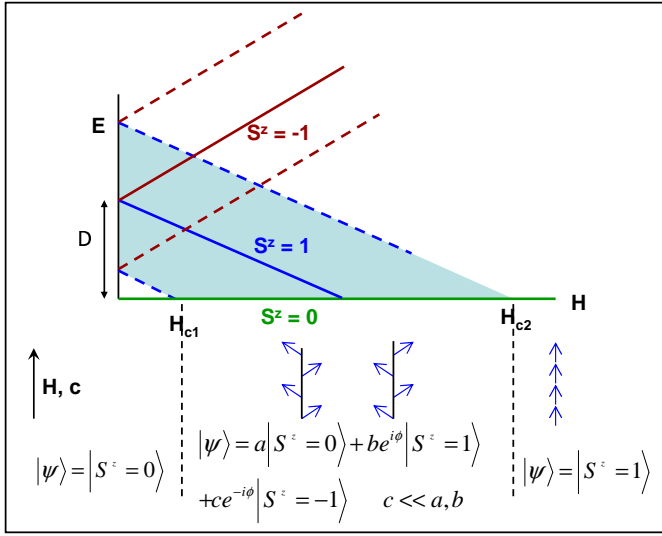


FIG. 2: Energy level diagram of DTN. The $S_z = \pm 1$ states are shown schematically as broad bands due to antiferromagnetic dispersion. The spins (blue arrows) form a disordered spin liquid with $S_z = 0$ below H_{c1} , then order in a canted AFM structure between H_{c1} and H_{c2} . Finally, above H_{c2} the spins polarize along the field direction. The ground state wave function $|\psi\rangle$ in these three regions is also indicated.

tion. As the field increases, the spins cant along the field direction until finally at H_{c2} , the spins polarize and the magnetization saturates. The magnetization along the c axis is shown overlaid on the phase diagram in Fig. 1. We should note that this description only holds for fields applied along the tetragonal c -axis. For fields in the a - b plane, the $S_z = 0$ groundstate mixes with a linear combination of the $S_z = \pm 1$ excited states and the resulting new set of eigenstates move apart with field, thus there is no level crossing and the system does not order.

Inelastic neutron scattering measurements in zero field⁹ indicate that the antiferromagnetic coupling is strongest along the Ni-Cl-Cl-Ni chains along the tetragonal c -axis, with the AFM exchange parameter $J_c =$

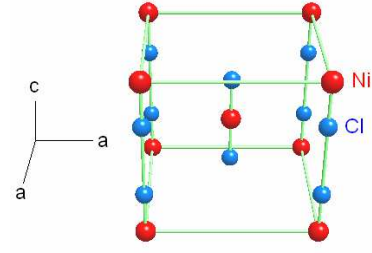


FIG. 3: Unit cell of tetragonal $\text{NiCl}_2\text{-4SC(NH}_2\text{)}_2$ showing Ni (red) and Cl (blue) atoms. Remaining atoms have been omitted for clarity.

1.74(3) K. The crystal structure of DTN is shown in Fig. 3. The coupling along the a -axis (and equivalently the b -axis), $J_a = J_b = 0.17(1)$ K, is significantly weaker, and no couplings were found to within the experimental resolution along the (1,1,1) direction. Thus the magnetic structure of this compound consists of semi-1D chains of Ni atoms that order three-dimensionally below 1.2 K in fields.

In DTN, the Bose statistics come about not because the spins are $S = 1$. In fact, theoretically BEC could be observed in a purely $S = 1/2$ magnetic system. Rather, the Bose statistics result from the fact that only the spins play a role in the Hamiltonian, and the atoms themselves are confined to lattice sites. The spin operators on different sites commute with each other, leading to Bose statistics.

The spin $S = 1$ system can be mapped into a gas of semi-hard-core bosons^{13,14,15} with no more than two bosons per site. The $|S_z = 1\rangle$, $|S_z = 0\rangle$ and $|S_z = -1\rangle$ states are mapped into the states with two, one and zero bosons respectively. The transverse component of the Heisenberg interaction is mapped into a hopping term while the longitudinal or Ising component becomes a nearest-neighbor repulsion. The single-ion anisotropy D generates an on-site repulsion and the magnetic field is mapped into a chemical potential. The resulting Hamiltonian in the particle representation is an extended Hubbard model for the semi-hard-core bosons. In the particle representation, the phase for $H < H_{c1}$ corresponds to the Mott insulator (one boson per site). When the chemical potential (magnetic field) reaches a critical value $H = H_{c1}$, the density ρ of bosons (magnetization) starts to increase continuously and the additional bosons relative to $\rho = 1$ form a BEC state at low enough temperature. This state is the particle version of the XY-antiferromagnet. When the chemical potential reaches a second critical value $H = H_{c2}$, all the sites are occupied by two bosons ($\rho = 2$) and the system enters a second Mott insulating phase that is the particle version of the fully saturated spin state.

The tetragonal crystal structure of DTN creates an approximate uniaxial symmetry (U(1) symmetry) of the spin system. This guarantees that the antiferromagnetic order for fields between H_{c1} and H_{c2} is XY-like, meaning

that there is no energetically favorable direction for the spins to point in the plane perpendicular to the applied field. The order parameter therefore acquires not only a magnitude but also a phase and the resulting Bose-Einstein Condensate exhibits spontaneous phase coherence.

There are several caveats to the idea of BEC in quantum spin systems. First of all, the uniaxial spin symmetry of the Hamiltonian is approximate. The square lattice of the crystal introduces anisotropy in the a - b plane as a result of spin-orbit coupling and dipole-dipole interactions.¹⁶ However, these effects generally occur at lower energy scales (often μK) and can thus be neglected at the temperatures of tens to hundreds of mK at which these quantum magnets are studied. In particular, no significant Dzyaloshinskii-Moriya interactions have been observed in electron-spin-resonance measurements of DTN.¹⁰

Thus, the Bose-Einstein condensation picture in quantum magnets is valid for the temperatures at which these compounds are studied, and more importantly it provides a way of understanding the observed physical behavior. The thermal phase transition in this system belongs to the $d = 3$ universality class of an XY antiferromagnet, where d is the number of spatial dimensions. However, the field-induced quantum phase transition belongs to the $D = 5$ ($d = 3, z = 2$) universality class where z is the dynamical exponent.

One of the key experimental signatures of the Bose-Einstein Condensation quantum critical point is the temperature-dependence of the critical field H_{c1} near $T = 0$. For a 3-D BEC, $H_{c1}(T) \propto T^\alpha$ where $\alpha = 3/2$. In contrast, the prediction for an Ising magnet is $\alpha = 2$, and for a 2-D BEC, $\alpha = 1$ (T corresponds to the Berezinskii-Kosterlitz-Thouless transition temperature in this case). In DTN, $H_{c1}(T)$ as $T \rightarrow 0$ has been investigated in detail by specific heat and magnetocaloric effect measurements.⁹ These data show that the expected power-law behavior $H_{c1}(T) - H_{c1}(0) \propto T^{3/2}$ for 3-D BEC is approached as $T \rightarrow 0$.⁹

In this work, we present magnetostriction measurements of DTN performed in a dilution refrigerator in a 20 T magnet system. The original motivation for these experiments, as mentioned in a previous work,⁹ was to account for a discrepancy between the observed and the predicted phase diagram. A semi-classical spin-wave approach predicted that $H_{c2} = 10.8$ T, in contrast to the observed value of $H_{c2} = 12.6$ T. In fact, it turns out that this discrepancy results from the presence of strong quantum fluctuations that limit the validity of a spin-wave approach. Taking fluctuations into account, the calculated value of H_{c2} is very close to the experimental one. Quantum Monte Carlo calculations are able to model both the $T-H$ phase diagram and the magnetization as a function of field very well.¹⁰ The magnetostriction is therefore not required to account for any deviations in the observed results.

Nevertheless, upon measuring magnetostriction in this

compound we have found significant field-induced lattice distortions in DTN, and these indicate that magnetoelastic coupling plays a role in this system. We find field-induced changes in the lattice parameters up to 0.025%, which is a relatively large effect. We also map the magnetic phase diagram as a function of magnetic field angle from the tetragonal c -axis.

II. RESULTS AND DISCUSSION

Magnetostriction measurements of single crystals of DTN were performed in a titanium dilatometer.⁷ The sample was mounted on a titanium base plate using Si vacuum grease. Length changes were monitored capacitatively with a Be-Cu spring-mounted titanium tip and the sample was protected from the tip with a .003" Ti foil. The dilatometer was mounted in a plastic rotator inside the ^3He - ^4He mixture of a top-loading dilution refrigerator, in a 20 T superconducting magnet system at the National High Magnetic Field Laboratory in Tallahassee, FL. Temperature was monitored with a ruthenium oxide thermometer, and capacitance changes were measured using a digital capacitance bridge operating at 5 kHz (Andeen-Hagerling model 2700A). Data is shown above $H = 1$ T, since flux jumps in the Nb_3Sn superconducting magnet affect the data at low fields.

New magnetization data for DTN is also presented. The longitudinal magnetization for $H||a$ was measured in a vibrating sample magnetometer (VSM) at 0.5 K.¹⁷

Magnetostriction data at 25 mK is shown in Fig. 4 for magnetic fields along the crystallographic c - and a -axes (top and bottom figures, respectively). For both field orientations, magnetostriction was measured along the a - and c -axes of the crystal, e.g. both perpendicular and parallel to the applied field.

For $H||c$ (Fig. 4 top,) changes in the length of the sample along the c axis, ΔL_c , clearly show features at the magnetic phase transitions at H_{c1} and H_{c2} . ΔL_c is nearly constant below H_{c1} and above H_{c2} , but varies dramatically in the region of antiferromagnetic order between H_{c1} and H_{c2} . Between $H_{c1} = 2.1$ T and ~ 5 T, L_c shrinks, and between 5 T and $H_{c2} = 12.5$ it expands, finally saturating at H_{c2} . This behavior is rather startling since the magnetization for $H||c$ increases roughly linearly with field between H_{c1} and H_{c2} . The longitudinal magnetization for $H||c$ is shown for comparison in Fig. 5. We interpret this nonmonotonic behavior in ΔL_c as arising from competing effects of antiferromagnetic and ferromagnetic components of the canted order. At H_{c1} the magnetic system orders purely antiferromagnetically in the a - b plane. Thus, by shrinking the distance between Ni atoms along the c -axis, the system can increase J_c and lower its magnetic energy. However, with increasing field, the spins cant along the field direction, increasing the ferromagnetic component. At some point it becomes more energetically favorable for the system to expand the c -axis thereby lowering the antiferromagnetic coupling J_c .

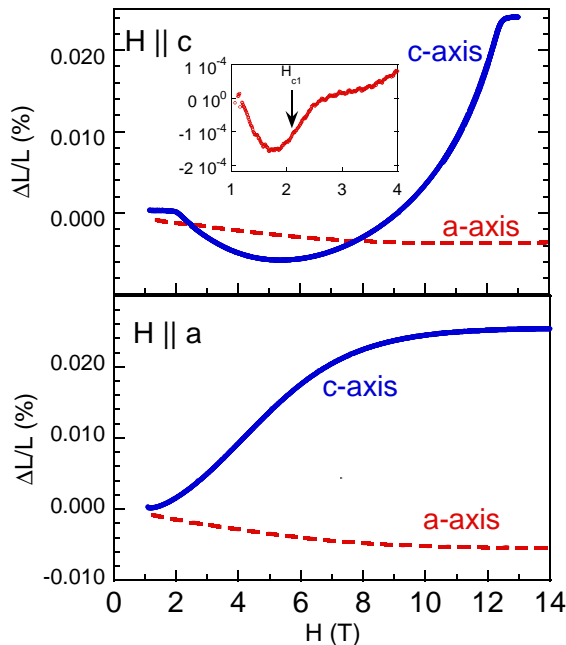


FIG. 4: Normalized percentage length change $\% \Delta L/L$ as a function of magnetic field measured along the crystallographic c -axis (solid blue lines) and a -axis (dashed red lines). Data is taken at 25 mK. The magnetic field is applied along the c -axis (top), and a -axis (bottom). The inset to the top figure is zoomed in on the feature at H_{c1} in $\% \Delta L/L_a$. A straight line has been subtracted from the data for clarity.

Finally, above H_{c2} the spins are saturated along the applied field direction and L_c remains roughly constant. The magnitude of the overall change in L_c between H_{c1} and H_{c2} is $\sim .025\%$. Such a distortion would be considered large in a metal and would most likely correspond to a structural phase transition. However, since DTN is a soft organic compound, a $.025\%$ distortion of the lattice parameters is reasonable.

The a -axis magnetostriction ΔL_a for $H||c$, shown as the red line in Fig. 4 (bottom), is smaller ΔL_c and H_{c1} is barely distinguishable at 2.1 T. The smaller magnetostriction along a makes sense since $J_a \ll J_c$. What is interesting is that ΔL_a doesn't follow the same non-monotonic behavior as ΔL_c . One might expect at first glance that ΔL_a should echo the same behavior as ΔL_c , just with a smaller magnitude. In reality, as the magnetic field becomes larger, ΔL_a doesn't reverse directions like ΔL_c does as the spins cant, but rather continues to decrease until it saturates near H_{c2} . This odd behavior could be due to the Poisson effect, e.g. volume-conserving forces typically present in tetragonal crystals cause L_a to contract as L_c expands. Thus at high fields, the a -axis lattice parameter responds more strongly to the distortions in the c -axis parameter than to magnetic forces from the antiferromagnetic coupling J_a .

For the other magnetic field direction, $H||a$, no magnetic order has been observed, and the system behaves

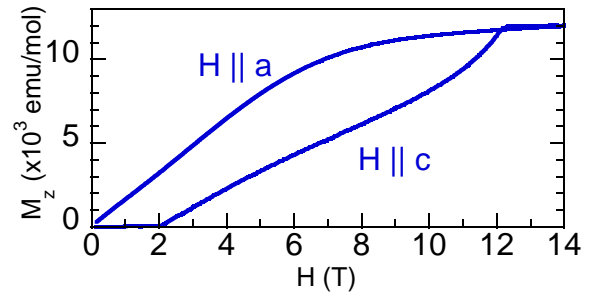


FIG. 5: Longitudinal magnetization of DTN for $H||c$ and $H||a$. The $H||c$ data is taken at 16 mK in a force magnetometer,¹² and the $H||a$ data is taken in a VSM at $T = 0.5$ K.

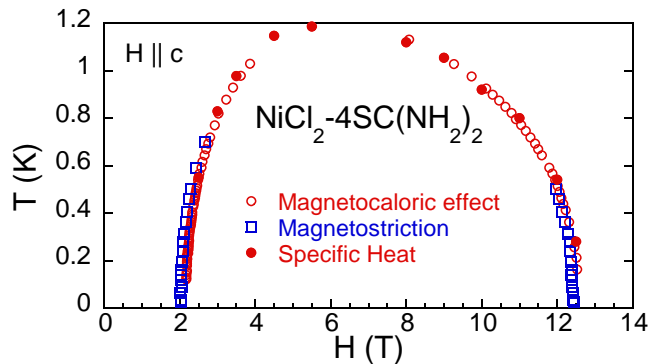


FIG. 6: Temperature T - Magnetic field H phase diagram for $H||c$ determined from magnetostriction, with the phase diagram from specific heat and magnetocaloric measurements shown for comparison⁹. The magnetostriction phase diagram (squares) is shifted to slightly lower fields, which may result from a slight pressure applied by the dilatometer.

paramagnetically. The magnetostriction shown in Fig. 4 (top) reflects this, and evolves smoothly with increasing magnetic field, eventually saturating at high fields. Similar to the $H||c$ case, L_c shows the strongest effect, and L_a moves in the opposite direction. The magnetization for $H||a$ is shown for comparison in Fig. 5.

The critical fields H_{c1} and H_{c2} can be extracted from the magnetostriction data ΔL_c for $H||c$. We take the peak in the second derivative of $\Delta L_c(H)$ to be the antiferromagnetic transition. We have used this technique to map the phase diagram as a function of temperature and field angle. The resulting temperature-field phase diagram is shown in Fig. 6, along with that determined from specific heat and magnetocaloric effect data for comparison.⁹ The phase diagram from magnetostriction closely tracks that determined from previous measurements, however, the phase transitions are shifted to slightly lower fields. The discrepancy between the phase diagrams cannot be accounted for by errors in the magnetic field centering, or by rotational misalignments. We assume therefore that this shift is due to pressure caused

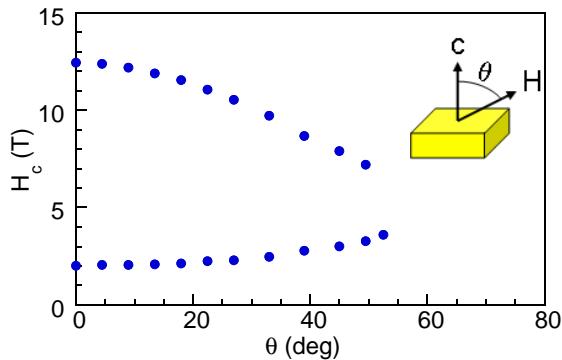


FIG. 7: Critical fields H_{c1} and H_{c2} at $T = 25$ mK as a function of field angle from the tetragonal c -axis determined from magnetostriction data.

by the spring-mounted dilatometer.

The critical fields H_{c1} and H_{c2} were also determined for different field angles θ to the tetragonal c -axis. The field-angle phase diagram is shown in Fig. 7. The region of antiferromagnetic order between H_{c1} and H_{c2} shrinks as θ increases, with antiferromagnetic order finally vanishing above $\theta = 55$ deg.

III. CONCLUSIONS

In conclusion, the compound $\text{NiCl}_2\cdot 4\text{SC}(\text{NH}_2)_2$ shows significant magnetoelastic effects, which indicate a strong coupling between the magnetic spin system and the lattice. As discussed previously, the observed magnetostriction data can be accounted for by magnetic forces resulting from the canted antiferromagnetic order, and by the Poisson effect that conserves the volume of the tetragonal crystal. The magnetostriction effects along the crystallographic c -axis are so large that the antiferromagnetic phase transition can be extracted from the data. The phase diagram as a function of temperature, field, and angle has been determined from the data, and agrees

roughly with specific heat and magnetocaloric effect measurements.

The original motivation for these measurements was to account for a discrepancy between spin-wave theory prediction of $H_{c2} = 10.85$ T and the observed value of $H_{c2} = 12.6$ T.⁹ The theory assumes constant values of J_a , J_c , and D , whereas a magnetostriction effect would cause J_a , J_c , and D vary with field.

However, this large discrepancy in H_{c2} has been mostly resolved by taking into account spin fluctuations. Nevertheless, small discrepancies between the theory and the experimental phase diagram and the magnetization vs field data still exist.¹⁰ These small discrepancies might still be accounted for by the structural distortions of the sample with field. The theoretical predictions for H_{c1} and H_{c2} are a 'best fit', obtained by varying the measured parameters D , J_a and J_c within their error bars. Thus both H_{c1} and H_{c2} show small discrepancies between theory and experiment. It is possible that a fit that preferentially matches H_{c1} would result in a larger discrepancy in H_{c2} , which is in fact accounted for by magnetostriction effects at high fields.

An important question that arises from these results is whether the tetragonal symmetry of the crystal is preserved or whether the magnetostriction effects induce a orthorhombic distortion. If the tetragonal symmetry of the crystal is compromised in high fields and the energy scale of these distortions is significant then the Bose-Einstein Condensation description of the magnetic phase transitions might no longer be valid. It would only be an accurate description at H_{c1} where the structural distortions go to zero. In order to investigate the possibility of structural distortions, resonant ultrasound measurements are in progress.

This work was supported by the DOE, the NSF, and Florida State University through the National High Magnetic Field Laboratory. V.S.Z. acknowledges support through the LANL Director-Funded Postdoctoral program and A.P.F. acknowledges support from CNPq (Conselho Nacional de Desenvolvimento Científico e Tecnológico, Brazil).

¹ M. H. Anderson, J. R. Ensher, M. R. Matthews, C. E. Wieman, and E. A. Cornell, *Science* **269**, 198 (1995).

² I. Affleck, *Phys. Rev. B* **43**, 3215 (1991).

³ T. Nikuni, M. Oshikawa, A. Oosawa, and H. Tanaka, *Phys. Rev. Lett.* **84**, 5868 (2000).

⁴ F. Yamada, T. Ono, M. Fujisawa, H. Tanaka, and T. Sakakibara, arXiv:cond-mat/0607439v1.

⁵ M. Jaime, V. F. Correa, N. Harrison, C. D. Batista, N. Kawashima, Y. Kazuma, G. A. Jorge, R. Stern, I. Heinmaa, S. A. Zvyagin, et al., *Phys. Rev. Lett.* **93**, 087203 (2004).

⁶ S. E. Sebastian, P. A. Sharma, M. Jaime, N. Harrison, V. Correa, L. Balicas, N. Kawashima, C. D. Batista, and I. R. Fisher, *Phys. Rev. B* **72**, 100404(R) (2005).

⁷ T. Radu, H. Wilhelm, V. Yushankhai, D. Kovrizhin, R. Coldea, Z. Tylczynski, T. Lühmann, and F. Steglich, *Phys. Rev. Lett.* **127202** (2005).

⁸ S. E. Sebastian, V. S. Zapf, N. Harrison, C. D. Batista, P. A. Sharma, M. Jaime, I. R. Fisher, and A. Lacerda, *Phys. Rev. Lett.* **96**, 189703 (2006).

⁹ V. S. Zapf, D. Zocco, B. R. Hansen, M. Jaime, N. Harrison, C. D. Batista, M. Kenzelmann, C. Niedermayer, A. Lacerda, and A. Paduan-Filho, *Phys. Rev. Lett.* **96**, 077204 (2006).

¹⁰ S. Zvyagin, J. Wosnitza, C. D. Batista, M. Tsukamoto, N. Kawashima, J. Krystek, V. S. Zapf, M. Jaime, N. F. Oliveira Jr., and A. Paduan-Filho, in progress.

¹¹ A. Paduan-Filho, R. D. Chirico, K. O. Joung, and R. L.

- Carlin, J. Chem. Phys. **74**, 4103 (1981).
- ¹² A. Paduan-Filho, X. Gratens, and N. F. Oliveira Jr., Phys. Rev. B **69**, 020405(R) (2004).
- ¹³ C. D. Batista and G. Ortiz, Phys. Rev. Lett. **86**, 1082 (2001).
- ¹⁴ C. D. Batista and G. Ortiz, Adv. Phys. **53**, 1 (2004).
- ¹⁵ K.-K. Ng and T.-K. Lee, cond-mat/0507663.
- ¹⁶ S. E. Sebastian, P. Tanedo, P. A. Goddard, S.-C. Lee, A. Wilson, S. Kim, S. Cox, R. D. McDonald, S. Hill, N. Harrison, et al., arXiv:cond-mat/0606244v1.
- ¹⁷ N. F. Oliveira Jr. and S. Foner, Rev. Sci. Instrum. **43**, 37 (1972).